

Polarization-dependent mass modifications of ϕ meson with finite momentum in nuclear matter

Ahmad Jafar Arifi^{1,2,*}, Philipp Gubler^{1,†} and Kazuo Tsushima^{3,‡}

¹*Advanced Science Research Center, Japan Atomic Energy Agency, Tokai, Ibaraki 319-1195, Japan*

²*Research Center for Nuclear Physics, The University of Osaka, Ibaraki, Osaka 567-0047, Japan*

³*Laboratório de Física Teórica e Computacional-LFTC,*

Programa de Pósgraduação em Astrofísica e Física Computacional,

Universidade Cidade de São Paulo, 01506-000 São Paulo, SP, Brazil

(Dated: March 18, 2026)

We investigate the in-medium properties of the ϕ meson with finite momentum, going beyond the commonly studied case at rest. In a nuclear medium, Lorentz invariance is broken, leading to distinct longitudinal and transverse polarization modes that evolve differently with density and momentum. Within an effective Lagrangian approach, we calculate the polarization-dependent mass shifts and width modifications of the ϕ meson arising from kaon loops and mean-field interactions. The divergent loop integrals are regulated using two different schemes: a covariant form factor and dimensional regularization. Our results show that the mass shift of the transverse polarization is independent of the ϕ -meson momentum, whereas that of the longitudinal polarization decreases quadratically with momentum. This difference originates from the coupling of the longitudinal mode to the vector mean field and derivative-type interactions in the self-energy. These effects have direct implications for experimental observables, especially for upcoming measurements at J-PARC, and provide a new prediction for experiments studying hadron dynamics in dense matter.

I. INTRODUCTION

Understanding hadron property changes in dense nuclear environments is a central challenge in nonperturbative quantum chromodynamics (QCD), as medium-induced modifications reflect changes in quark and gluon dynamics and the reduction of the quark condensate, signaling partial restoration of chiral symmetry (in light quark sector) [1–3]. Light vector mesons are especially important, since their masses and spectral functions directly probe such effects. Early studies, notably Brown-Rho scaling [4] and QCD sum rules (QCDSR) [5], predicted downward mass shifts with increasing density, triggering extensive theoretical and experimental efforts. Among them, the ϕ meson is particularly notable: its dominant $s\bar{s}$ structure and narrow vacuum width make it a relatively clean probe of in-medium dynamics, less affected by conventional hadronic many-body effects than the ρ and ω mesons.

The in-medium properties of the ϕ meson is known to be sensitive to the strange sigma term of the nucleon [6], $\sigma_{sN} \equiv m_s \langle N | \bar{s}s | N \rangle$, which controls the density dependence of the strange quark condensate [7, 8]. Lattice QCD has put also constraints on σ_{sN} [9–14], although there is a tension with the extracted value from experiments. Studies of the ϕN interaction [15–18] also reveal coupled-channel dynamics, hidden strangeness, and near-threshold effects, motivating searches for ϕ -nucleus

bound states [19, 20]. Furthermore, transport simulations [21] have been performed to connect theory to proton- and photo-nuclear reaction related observables [22–25], while in-medium ϕ mesons also impact heavy-ion collisions [26–33].

Experimentally, measurements at various facilities have provided evidence for density-dependent modifications of the ϕ meson spectral function [34–40]. While dilepton decays offer a clean and direct probe of in-medium effects, their small branching ratio restricts statistical precision; in contrast, the $K\bar{K}$ decay channel provides higher yields but suffers from strong final-state interactions. In particular, the KEK-E325 experiment observed a downward mass shift and substantial broadening via dilepton measurements [25, 35]. However, existing data remain partially inconsistent [25], preventing a definitive conclusion. Ongoing and future experiments at J-PARC, in particular, the E16 and E88/Sa ϕ re programs, aim to significantly improve precision [41–45]. Additional experimental programs on the ϕ meson are also planned at GSI [46].

On the theoretical side, most studies have focused on the ϕ meson at rest using various approaches, e.g., [47–56], generally predicting a downward mass shift accompanied by a significant broadening of the decay width in nuclear matter. However, in realistic experiments [25, 35], ϕ mesons carry finite momentum in a Lorentz symmetry broken environment, generating distinct longitudinal and transverse polarization modes with different in-medium evolution. Such polarization-dependent effects represent a qualitatively new aspect of vector meson dynamics and have been explored mainly within QCDSR analyses [57, 58], while systematic studies using other effective hadronic models remain limited.

In this work, we study the in-medium ϕ meson prop-

* aj.arifi01@gmail.com

† gubler.philipp@jaea.go.jp; philipp.gubler1@gmail.com

‡ kazuo.tsushima@cruzeirodosul.edu.br;

kazuo.tsushima@gmail.com

erties at finite momentum, with particular emphasis on the ϕ -polarization effects. To this end, we investigate the in-medium ϕ meson self-energy arising from kaon loops within an effective Lagrangian approach [47, 53, 55], combined with in-medium kaon inputs from the quark-meson coupling (QMC) model [59]. While the previous study [53] employed three-momentum form factors to evaluate the kaon loops, here we adopt two Lorentz invariant regularization schemes, covariant form factors and dimensional regularization, to consistently extend the analysis to finite momentum without introducing artificial Lorentz breaking effects.

Our results reveal a quadratic mass decrease with increasing momentum in the longitudinal mode, driven by vector mean fields and derivative interactions, while the transverse-mode mass remains insensitive. The behavior of the longitudinal-mode mass is consistent with QCDSR predictions [58], whereas the transverse-mode mass exhibits a qualitatively different trend. These differences can be resolved in future experiments and provide clear experimental signatures, potentially accessible through angular correlations in the $\phi \rightarrow K\bar{K}$ decay channel [60]. The planned J-PARC E88/Sa ϕ re experiment offers a promising opportunity to directly observe polarization-dependent mass splitting [45].

This paper is organized as follows. In Sec. II, we introduce the formalism for the self-energy of the ϕ meson, including its vacuum contribution, and describe the in-medium modifications of the kaon mass and energy in the QMC model, which provide essential inputs for the self-energy calculation. Section III presents the evaluation of the ϕ meson self-energy using two different regularization schemes. The model parameters employed in the present study are discussed in Sec. IV. The numerical results and their detailed analysis are given in Sec. V. Finally, our conclusions and outlook are summarized in Sec. VI. Technical details of the form-factor and dimensional regularization methods are provided in Apps. A and B, respectively, where analytic expressions are derived to ensure the correctness of the numerical calculations.

II. SELF-ENERGY OF ϕ MESON

In this work, we study in-medium modifications of the ϕ -meson mass and width in the laboratory frame, as relevant for J-PARC and other experiments [41–45]. Thus, we focus on medium effects on the ϕ -meson self-energy at finite momentum $p^\mu = (p^0, 0, 0, |\mathbf{p}|)$, where the kaon inside the loop is modified. In a nuclear medium, Lorentz symmetry is broken due to the existence of a preferred frame defined by the medium four-velocity: $u^\mu = (1, 0, 0, 0)$, leading to a separation between transverse and longitudinal polarization modes. The self-energy tensor $\Pi^{\mu\nu}$ can then be given as [61]

$$\Pi^{\mu\nu}(p) = P_T^{\mu\nu}\Pi^T(p) + P_L^{\mu\nu}\Pi^L(p), \quad (1)$$

where the splitting vanishes in the ϕ -meson rest frame, in which both modes become degenerate. Here, $P_T^{\mu\nu}$ and $P_L^{\mu\nu}$ are the transverse and longitudinal projectors which satisfy

$$P_T^{\mu\nu} + P_L^{\mu\nu} = -g^{\mu\nu} + \frac{p^\mu p^\nu}{p^2}, \quad (2)$$

and can be used to separate tensor structures in in-medium self-energies and propagators according to their polarization modes. Both projectors satisfy the transversality conditions $P_{L/T}^{\mu\nu}p_\mu = 0$ and the following condition $P_{L\mu}^\mu = \frac{1}{2}P_{T\mu}^\mu = -1$. The projectors have also the property $P_{L/T}^{\mu\sigma}P_{\sigma\nu}^{L/T} = -P_{\nu,L/T}^\mu$ and $P_T^{\mu\sigma}P_{\sigma\nu}^L = 0$. The transverse projector can be expressed as $P_T^{0i} = P_T^{i0} = 0$ and

$$P_T^{ij} = \delta^{ij} - \frac{p^i p^j}{p^2}, \quad (3)$$

while the longitudinal polarization projector can then be computed as

$$P_L^{\mu\nu} = -g^{\mu\nu} + \frac{p^\mu p^\nu}{p^2} - P_T^{\mu\nu}. \quad (4)$$

The longitudinal and transverse self-energy of the ϕ meson can therefore be computed as

$$\Pi_T(p) = \frac{1}{2}P_{\mu\nu}^T \Pi^{\mu\nu}(p), \quad \Pi_L(p) = P_{\mu\nu}^L \Pi^{\mu\nu}(p). \quad (5)$$

A. Effective Lagrangian approach

The ϕ -meson self-energy in nuclear matter is evaluated in an effective Lagrangian approach [47, 53]. The dominant interaction is provided by the $\phi K\bar{K}$ coupling,

$$\mathcal{L}_{\phi K\bar{K}} = ig_\phi \phi^\mu [\bar{K}(\partial_\mu K) - (\partial_\mu \bar{K})K], \quad (6)$$

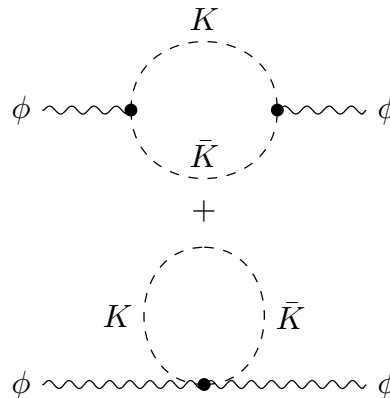


FIG. 1. Self-energy of the ϕ meson through: (top) a $K\bar{K}$ loop term and (bottom) a contact four-point coupling term.

together with the corresponding four-point $\phi\phi K\bar{K}$ interaction,

$$\mathcal{L}_{\phi\phi K\bar{K}} = g_\phi^2 \phi^\mu \phi_\mu \bar{K} K, \quad (7)$$

where the kaon and antikaon fields are written as

$$K = \begin{pmatrix} K^+ \\ K^0 \end{pmatrix}, \quad \bar{K} = (K^- \quad \bar{K}^0). \quad (8)$$

The interaction terms in Eqs. (6) and (7) arise naturally from a gauged kaon kinetic Lagrangian, in which the ϕ meson is introduced as a vector gauge field [47, 53]. Starting from the free kaon Lagrangian and promoting the ordinary derivative to a covariant one, $\partial_\mu \rightarrow D_\mu = \partial_\mu + ig_\phi \phi_\mu$, the expansion of the gauged kinetic term generates simultaneously the three-point $\phi K\bar{K}$ vertex and the four-point $\phi\phi K\bar{K}$ interaction. As a consequence, these couplings are not independent but are constrained by local gauge invariance.

At the level of the ϕ -meson self-energy, the three-point interaction gives rise to the kaon–antikaon loop contribution, while the four-point coupling term generates a contact (to be noted by “con” hereafter) diagram as shown in Fig. 1. Their combined contribution

$$\Pi_{\text{total}}^{\mu\nu}(p) = \Pi_{\text{loop}}^{\mu\nu}(p) + \Pi_{\text{con}}^{\mu\nu}(p) \quad (9)$$

ensures the transversality of the vector-meson self-energy,

$$p_\mu \Pi_{\text{total}}^{\mu\nu}(p) = 0. \quad (10)$$

The $\Pi^{\mu\nu}$ computed from a kaon loop and a contact term in Fig. 1 can be expressed as [47, 53]

$$\Pi_{\text{loop}}^{\mu\nu}(p) = 2ig_\phi^2 \int \frac{d^4 q}{(2\pi)^4} \frac{S_{\text{loop}}^{\mu\nu}}{D_K(q)D_{\bar{K}}(p-q)}, \quad (11)$$

$$\Pi_{\text{con}}^{\mu\nu}(p) = 2ig_\phi^2 \int \frac{d^4 q}{(2\pi)^4} \frac{S_{\text{con}}^{\mu\nu}}{D_K(q)}, \quad (12)$$

where q is the kaon four-momentum and the factor two is coming from the charged and neutral kaon loop [53]. Here, we assume that the kaon is a stable particle and has no width. The numerators are given by

$$S_{\text{loop}}^{\mu\nu} = (2q-p)^\mu (2q-p)^\nu, \quad S_{\text{con}}^{\mu\nu} = -2g^{\mu\nu}, \quad (13)$$

while the kaon and antikaon propagators are expressed by

$$D_K(q) = q^2 - m_K^2 + i\epsilon, \quad (14)$$

$$D_{\bar{K}}(p-q) = (p-q)^2 - m_K^2 + i\epsilon, \quad (15)$$

where $m_K (= m_{\bar{K}})$ is the kaon scalar mass. Projecting onto the transverse and longitudinal polarization modes ($\lambda = T, L$), we obtain

$$\Pi_{\text{total}}^\lambda(p) = 2ig_\phi^2 \int \frac{d^4 q}{(2\pi)^4} \left(\frac{\mathcal{O}_{\text{loop}}^\lambda}{D_K D_{\bar{K}}} + \frac{\mathcal{O}_{\text{con}}^\lambda}{D_K} \right), \quad (16)$$

where the operator \mathcal{O}_λ is defined by

$$\mathcal{O}_L = P_{\mu\nu}^L S^{\mu\nu}, \quad \mathcal{O}_T = \frac{1}{2} P_{\mu\nu}^T S^{\mu\nu}. \quad (17)$$

B. In-medium modifications

In nuclear matter, the ϕ -meson self-energy can be written as [53]

$$\Pi_{\text{total}}^\lambda(p) = 2ig_\phi^2 \int \frac{d^4 q}{(2\pi)^4} \left(\frac{\mathcal{O}_{\text{loop}}^{\lambda*}}{D_K^* D_{\bar{K}}^*} + \frac{\mathcal{O}_{\text{con}}^{\lambda*}}{D_K^*} \right), \quad (18)$$

where

$$D_K^* = (q^{0*})^2 - \mathbf{q}^2 - m_K^{*2} + i\epsilon, \quad (19)$$

$$D_{\bar{K}}^* = (p^{0*} - q^{0*})^2 - (\mathbf{p} - \mathbf{q})^2 - m_K^{*2} + i\epsilon, \quad (20)$$

with the scalar mean field affecting the kaon mass,

$$m_K^* \equiv m_K - V_\sigma, \quad (21)$$

while the vector mean field affecting the kaon energy, modifying the dispersion relation

$$q^{0*} = q^0 + V_\omega, \quad (p - q)^{0*} = (p - q)^0 - V_\omega. \quad (22)$$

Note that we denote all in-medium quantities with an asterisk. In the lab frame, we can do a variable shift,

$$q^0 \rightarrow q^0 - V_\omega, \quad (23)$$

and can obtain the same formal expression as in Eq. (18), with operators shifted as

$$\mathcal{O}_{\text{loop}}^{\lambda*} \rightarrow \mathcal{O}_{\text{loop}}^{\lambda*}(p, q^0 - V_\omega). \quad (24)$$

Note that, the operator $\mathcal{O}_{\text{loop}}^{\lambda*}$ can depend explicitly on q^0 , and this dependence is modified by the vector mean field V_ω . As a consequence, the transverse and longitudinal polarization modes become separated. However, $\mathcal{O}_{\text{con}}^{\lambda*}$ does not depend on q^0 and therefore is not affected by V_ω . After the shift in Eq. (23), the in-medium propagators can be defined without V_ω dependence as

$$D_K^* = (q^0)^2 - \mathbf{q}^2 - m_K^{*2} + i\epsilon, \quad (25)$$

$$D_{\bar{K}}^* = (p^0 - q^0)^2 - (\mathbf{p} - \mathbf{q})^2 - m_K^{*2} + i\epsilon, \quad (26)$$

and this notation will be used throughout this work.

C. In-medium ϕ mass and spectral functions

Once the ϕ self-energy $\Pi(p)$ is obtained, the respective in-medium mass and decay width can be determined. When the kinematic condition $m_\phi^* > 2m_K^*$ is satisfied, the self-energy develops an imaginary part, corresponding to the opening of the $\phi \rightarrow K\bar{K}$ decay channel in the medium.

The in-medium mass of the ϕ meson is then determined from the real part of the self-energy through

$$m_\phi^{*2} = (m_\phi^0)^2 + \text{Re} \Pi(E_\phi^{*2}, \mathbf{p}^2), \quad (27)$$

where m_ϕ^0 denotes the bare ϕ -meson mass fixed in vacuum. The corresponding in-medium decay width for the $\phi \rightarrow K\bar{K}$ process is given by the imaginary part of the self-energy,

$$\Gamma_\phi^* = -\frac{1}{E_\phi^*} \text{Im} \Pi(E_\phi^{*2}, \mathbf{p}^2), \quad (28)$$

with $E_\phi^* = \sqrt{m_\phi^{*2} + \mathbf{p}^2}$. Note that by defining $\gamma = E_\phi^*/m_\phi^*$, the in-medium decay width can be rewritten as $\Gamma_\phi^* = \Gamma_\phi^{*0}/\gamma$. While Γ_ϕ^{*0} captures the dynamical effects of the medium on the ϕ -meson, the γ factor accounts for the kinematical effect, originating from Lorentz time dilation, which suppresses the observed width in the moving frame. This also implies that a fast ϕ meson has a longer effective lifetime and is more likely to decay outside the nucleus, resulting in smaller medium effects on the observables. Larger modifications, in contrast, are observed experimentally for slow ϕ mesons [25, 35].

Equations (27) and (28) are solved self-consistently using the in-medium kaon mass m_K^* to obtain the ϕ meson mass shift and width. In Sec. III, we evaluate the self-energy using two different regularization schemes in order to assess the robustness and model dependence of our results.

To make connection with experiment, it is useful to introduce the in-medium ϕ -meson spectral functions using a Breit-Wigner parametrization [58],

$$A_\phi^\lambda(s, \mathbf{p}^2) = \frac{C_\lambda}{\pi} \frac{\sqrt{s}\Gamma_\phi^*(\mathbf{p})}{(s - m_\phi^{*2}(\mathbf{p}))^2 + s\Gamma_\phi^{*2}(\mathbf{p})}. \quad (29)$$

The normalization constant C_λ is determined by the condition

$$\int_0^\infty ds A_\phi^\lambda(s, \mathbf{p}^2) = 1. \quad (30)$$

Since most dilepton measurements have so far not been able to resolve individual polarization states, it is natural to introduce a polarization-averaged spectral function, defined as

$$A_\phi^{\text{ave}}(s, \mathbf{p}^2) = \frac{1}{3} \left[A_\phi^L(s, \mathbf{p}^2) + 2A_\phi^T(s, \mathbf{p}^2) \right]. \quad (31)$$

This polarization averaging provides a practical connection between theoretical predictions, transport calculations, and dilepton measurements [23].

D. In-medium kaon mass

The modification of the kaon mass and energy in nuclear matter is an important input in our study. The kaon mass and energy in medium are evaluated in the QMC model [59], which was proposed by Guichon [62] and has been successfully applied to describe both infinite nuclear matter and finite nuclei (see Refs. [63, 64] for

reviews). Here we summarize only the elements relevant to the present work.

In the QMC model, nuclear matter is treated in its rest frame within the mean-field (Hartree) approximation, where the scalar and vector meson fields are spatially constant. The light quarks $q = (u, d)$ inside a hadron bag couple directly to these mean fields, while the strange quark remains unaffected. Here we assume SU(2) symmetry for the light quarks ($m_q = m_u = m_d$). The corresponding Dirac equations for the quark fields in symmetric nuclear matter,

$$[i\cancel{\partial} - m_q^* \mp \gamma^0 V_\omega^q] \begin{pmatrix} \psi_q \\ \psi_{\bar{q}} \end{pmatrix} = 0, \quad [i\cancel{\partial} - m_s] \begin{pmatrix} \psi_s \\ \psi_{\bar{s}} \end{pmatrix} = 0, \quad (32)$$

lead to an effective light-quark mass

$$m_q^* \equiv m_q - V_\sigma^q. \quad (33)$$

Since we restrict our study to symmetric nuclear matter, the contribution from the ρ meson mean field can be neglected. The mean-field potentials are then written as

$$V_\sigma^q = g_\sigma^q \sigma, \quad V_\omega^q = g_\omega^q \omega, \quad (34)$$

where g_σ^q and g_ω^q are the corresponding quark-meson coupling constants.

The normalized static solution for a ground-state quark or antiquark of flavor f in a kaon K can be expressed as

$$\psi_f(x) = N_f e^{-i\epsilon_f t/R_K^*} \psi_f(\mathbf{r}), \quad (35)$$

where N_f is the normalization factor and $\psi_f(\mathbf{r})$ denotes the spatial and spinor wave function. The in-medium bag radius, R_K^* , is determined by imposing the stability condition on the hadron mass with respect to variations of the radius.

The corresponding eigenenergies (in units of $1/R_K^*$) take the form

$$\begin{pmatrix} \epsilon_u \\ \epsilon_{\bar{u}} \end{pmatrix} = \Omega_q^* \pm R_K^* V_\omega^q, \quad \begin{pmatrix} \epsilon_d \\ \epsilon_{\bar{d}} \end{pmatrix} = \Omega_q^* \pm R_K^* V_\omega^q, \quad (36)$$

and $\epsilon_s = \epsilon_{\bar{s}} = \Omega_s$. Then, the excitation energy of K and \bar{K} mesons with zero momenta are given by

$$\begin{pmatrix} E_{K^+} \\ E_{K^-} \end{pmatrix} = m_K^* \pm V_\omega, \quad \begin{pmatrix} E_{K^0} \\ E_{\bar{K}^0} \end{pmatrix} = m_K^* \pm V_\omega. \quad (37)$$

In a constant vector field, the Lorentz invariance of the dispersion relation for the K and \bar{K} mesons moving with momentum \mathbf{q} are given by [59, 65]

$$\begin{pmatrix} E_{K^+}(\mathbf{q}) \\ E_{K^-}(\mathbf{q}) \end{pmatrix} = \sqrt{m_K^{*2} + \mathbf{q}^2} \pm V_\omega, \quad (38)$$

$$\begin{pmatrix} E_{K^0}(\mathbf{q}) \\ E_{\bar{K}^0}(\mathbf{q}) \end{pmatrix} = \sqrt{m_K^{*2} + \mathbf{q}^2} \pm V_\omega, \quad (39)$$

which is useful for the calculation of the in-medium $K\bar{K}$ loop. Here, the background nuclear matter is treated as static, uniform, and at rest. In such a medium the vector field is generated by nucleons that are, on average, at rest, so that the expectation value of the vector mean field remains purely time-like.

The in-medium kaon mass is then calculated as

$$m_K^* = \sum_{j=q,\bar{s}} \frac{n_j \Omega_j^* - z_K}{R_K^*} + \frac{4\pi}{3} R_K^{*3} B, \quad (40)$$

where z_K accounts for the center-of-mass and gluon fluctuation corrections, and B is the bag constant. The in-medium mass is obtained by imposing the stability condition

$$\frac{dm_K^*}{dR_K^*} = 0. \quad (41)$$

Here, the quark eigenenergies are

$$\Omega_q^* = \Omega_{\bar{q}}^* = \sqrt{x_q^2 + (R_K^* m_q^*)^2}, \quad (42)$$

$$\Omega_s^* = \Omega_{\bar{s}}^* = \sqrt{x_s^2 + (R_K^* m_s^*)^2}, \quad (43)$$

where $x_{q,s}$ are the lowest bag eigenfrequencies, and $n_q(n_{\bar{q}})$ denote the numbers of quarks (antiquarks) of flavors q and s . After a self-consistent calculation, the in-medium kaon mass can be parameterized as

$$m_K^* \equiv m_K - V_\sigma. \quad (44)$$

We note that this kaon mass remains unchanged in the moving kaon frame due to its scalar nature.

III. REGULARIZATION SCHEMES

In this work, we consider two different regularization schemes to evaluate the ϕ -meson self-energy. We do not consider the three-momentum form factor employed for the zero-momentum case in the previous work of Ref. [53], because this procedure explicitly breaks Lorentz covariance, and is hence not suitable for the finite-momentum case, which is the focus of the present study. To overcome this limitation, we employ a covariant form factor as well as dimensional regularization [47]. Using two different schemes allows us to check the scheme dependence and assess the robustness of our results.

A. Form factor regularization

We first consider a covariant form factor with a multiple Ansatz to regulate the self-energy of the ϕ meson

shown in Fig. 1. The total self-energy is given by

$$\begin{aligned} \Pi_{\text{total}}^\lambda(p) &= 2ig_\phi^2 \int \frac{d^4q}{(2\pi)^4} \left(\frac{\mathcal{O}_{\text{loop}}^{\lambda*}}{D_K^* D_{\bar{K}}^*} + \frac{\mathcal{O}_{\text{con}}^{\lambda*}}{D_K^*} \right) F(q, \Lambda) \\ &= 2ig_\phi^2 (\Lambda^2 - m_K^{*2})^2 \\ &\quad \times \int \frac{d^4q}{(2\pi)^4} \left(\frac{\mathcal{O}_{\text{loop}}^{\lambda*}}{D_\Lambda^2 D_K^* D_{\bar{K}}^*} + \frac{\mathcal{O}_{\text{con}}^{\lambda*}}{D_\Lambda^2 D_K^*} \right), \end{aligned} \quad (45)$$

with $D_\Lambda = q^2 - \Lambda^2 + i\epsilon$. The regulator is chosen as

$$F(q, \Lambda) = \frac{(\Lambda^2 - m_K^{*2})^2}{(q^2 - \Lambda^2 + i\epsilon)^2}, \quad (46)$$

where the cutoff parameter Λ is assumed to be independent of the nuclear density. As mentioned before, the total contribution can be decomposed into loop and contact terms, $\Pi_{\text{total}}^\lambda = \Pi_{\text{loop}}^\lambda + \Pi_{\text{con}}^\lambda$.

The operators appearing in the numerator, defined in Eq. (17), are evaluated as

$$\mathcal{O}_{\text{loop}}^{T*} = \frac{1}{2} P_{\mu\nu}^T (2q-p)^\mu (2q-p)^\nu = 2q_\perp^2, \quad (47)$$

$$\begin{aligned} \mathcal{O}_{\text{loop}}^{L*} &= P_{\mu\nu}^L (2q-p)^\mu (2q-p)^\nu \\ &= \frac{4}{m_\phi^{*2}} ([q^0 - V_\omega] |\mathbf{p}| - q^z E_\phi^*)^2, \end{aligned} \quad (48)$$

$$\mathcal{O}_{\text{con}}^{L(T)*} = \frac{1}{2} P_{\mu\nu}^T (-2g^{\mu\nu}) = P_{\mu\nu}^L (-2g^{\mu\nu}) = 2, \quad (49)$$

where a variable shift of q^0 , given in Eq. (23), has been performed. The operators for the transverse and longitudinal modes differ in structure. For the transverse mode, the operator does not depend on the ϕ -meson three-momentum $|\mathbf{p}|$, whereas for the longitudinal mode it exhibits an explicit momentum dependence, together with the vector mean field V_ω . The absence of momentum dependence in the transverse operator follows from $\mathbf{p}_\perp = 0$, such that only the longitudinal momentum component is nonvanishing. By contrast, the operator for the contact term is identical for both longitudinal and transverse projectors.

After introducing the Feynman parameterization, Wick rotation, and Euclidean integration, the total self-energies for the transverse and longitudinal modes are given by

$$\Pi_{\text{total}}^T(p) = N \int_0^1 dx \left[\int_0^{1-x} dy \frac{(1-x-y)}{C} - \frac{x}{E} \right], \quad (50)$$

$$\begin{aligned} \Pi_{\text{total}}^L(p) &= N \int_0^1 dx \left[\int_0^{1-x} dy (1-x-y) \right. \\ &\quad \left. \times \left(\frac{1}{C} - \frac{2|\mathbf{p}|^2 V_\omega^2}{m_\phi^{*2} C^2} \right) - \frac{x}{E} \right], \end{aligned} \quad (51)$$

where $N = g_\phi^2 (\Lambda^2 - m_K^{*2})^2 / 4\pi^2$, with the denominator factors given by

$$C = x(1-x)m_\phi^{*2} - (x+y)m_K^{*2} - (1-x-y)\Lambda^2, \quad (52)$$

$$E = x\Lambda^2 - (1-x)m_K^{*2}. \quad (53)$$

Note that the contact term corresponds to the contribution proportional to E , while the loop term involves C . To compute the real part, the integrals are evaluated using the principal-value calculation, where the numerical implementation avoids singularities by smearing, for example through a Breit–Wigner form,

$$\frac{1}{C} \rightarrow \frac{C}{C^2 + \Gamma^2}, \quad \frac{1}{C^2} \rightarrow \frac{C^2 - \Gamma^2}{(C^2 + \Gamma^2)^2}, \quad (54)$$

where Γ is a small regulator parameter. An explicit analytical calculation is also possible. The details of calculation and analytical expressions for these integrals are provided in App. A.

While the real part depends on the regulator Λ , the imaginary part is given by

$$\text{Im } \Pi_{\text{total}}^T(p) = -\frac{g_\phi^2}{24\pi} m_\phi^{*2} \beta^3, \quad (55)$$

$$\text{Im } \Pi_{\text{total}}^L(p) = -\frac{g_\phi^2}{24\pi} m_\phi^{*2} \beta^3 \left(1 + \frac{12 V_\omega^2 |\mathbf{p}|^2}{\beta^2 m_\phi^{*4}} \right), \quad (56)$$

with $\beta = \sqrt{1 - 4m_K^{*2}/m_\phi^{*2}}$. The imaginary part arises solely from the loop diagram, whereas the contact term contributes only to the real part. Putting into Eq. (28), the decay width can be explicitly expressed by

$$\Gamma_\phi^{*T} = \frac{g_\phi^2}{24\pi\gamma} m_\phi^{*2} \beta^3, \quad (57)$$

$$\Gamma_\phi^{*L} = \frac{g_\phi^2}{24\pi\gamma} m_\phi^{*2} \beta^3 \left(1 + \frac{12 V_\omega^2 |\mathbf{p}|^2}{\beta^2 m_\phi^{*4}} \right), \quad (58)$$

where the γ factor has been included.

B. Dimensional Regularization

We now turn to dimensional regularization, which was used for instance in Ref. [47]. The ϕ -meson self-energy can be written as

$$\Pi_{\text{total}}^\lambda(p) = 2ig_\phi^2 \int \frac{d^4q}{(2\pi)^4} \left(\frac{\mathcal{O}_{\text{loop}}^{\lambda*}}{D_K^* D_{\bar{K}}^*} + \frac{\mathcal{O}_{\text{con}}^{\lambda*}}{D_K^*} \right), \quad (59)$$

without introducing an explicit form factor.

For the contact term, the self-energy is identical for transverse and longitudinal polarizations and is given by

$$\Pi_{\text{con}}^\lambda(p) = 4ig_\phi^2 \int \frac{d^4q}{(2\pi)^4} \frac{1}{D_K^*}, \quad (60)$$

where we have used $\mathcal{O}_{\text{con}}^{\lambda*} = 2$, as in Eq. (49). After applying the Feynman parameterization and momentum shift to complete the square, the self-energy for the loop contribution can be expressed as

$$\Pi_{\text{loop}}^\lambda(p) = 2ig_\phi^2 \int_0^1 dx \int \frac{d^4q}{(2\pi)^4} \frac{\mathcal{O}_{\text{loop}}^{\lambda*}}{D_\Delta^{*2}}, \quad (61)$$

where $D_\Delta^* = q^2 - \Delta^* + i\epsilon$ and $\Delta^* = m_K^{*2} - x(1-x)m_\phi^{*2}$. The explicit forms of the operators for the transverse and longitudinal modes are the same as in Eqs. (47) and (48), respectively.

Including both the loop and contact contributions, the transverse self-energy can be written as

$$\Pi_{\text{total}}^T(p) = 4ig_\phi^2 \int \frac{d^d q}{(2\pi)^d} \left(\int_0^1 dx \frac{P_{\mu\nu}^T q^\mu q^\nu}{D_\Delta^{*2}} + \frac{1}{D_K^*} \right), \quad (62)$$

where, in d dimensions, we have used the identity $\mathbf{q}_\perp^2 = P_{\mu\nu}^T q^\mu q^\nu$. The momentum integrals are evaluated using dimensional regularization in $d = 4 - \epsilon$ dimensions. Keeping only finite terms, the renormalized transverse self-energy reads

$$\Pi_{\text{total}}^T(p) = -\frac{g_\phi^2}{4\pi^2} \int_0^1 dx \left(\Delta^* \ln \frac{\Delta^*}{\mu^2} - m_K^{*2} \ln \frac{m_K^{*2}}{\mu^2} - a(\mu) \frac{m_\phi^2}{6} \right), \quad (63)$$

where the first two terms arise from the loop and contact contributions, respectively. Here μ denotes the renormalization scale, and $a(\mu)$ is a dimensionless subtraction constant that absorbs the ultraviolet divergence. The factor $m_\phi^2/6$ originates from the combined loop and contact contributions.

For the longitudinal mode, the loop contribution is given by

$$\Pi_{\text{loop}}^L(p) = \frac{8ig_\phi^2}{m_\phi^{*2}} \int_0^1 dx \int \frac{d^4q}{(2\pi)^4} \frac{\left([q^0 - V_\omega] |\mathbf{p}| - q^z E_\phi^* \right)^2}{D_\Delta^{*2}}. \quad (64)$$

By adding the contact contributions and following procedures similar to those used for the transverse mode, we obtain

$$\Pi_{\text{total}}^L(p) = -\frac{g_\phi^2}{4\pi^2} \int_0^1 dx \left[\Delta^* \ln \frac{\Delta^*}{\mu^2} - m_K^{*2} \ln \frac{m_K^{*2}}{\mu^2} - 2V_\omega^2 \frac{|\mathbf{p}|^2}{m_\phi^{*2}} \left(\ln \frac{\Delta^*}{\mu^2} + 1 \right) - a(\mu) \frac{m_\phi^2}{6} \right]. \quad (65)$$

The details of calculations and analytic expressions are provided in App. B.

While the real part depends on the renormalization scale μ and the subtraction constant $a(\mu)$, the imaginary parts of the transverse and longitudinal self-energies are again independent of the regularization scheme and are given by

$$\text{Im } \Pi_{\text{total}}^T(p) = -\frac{g_\phi^2}{24\pi} m_\phi^{*2} \beta^3, \quad (66)$$

$$\text{Im } \Pi_{\text{total}}^L(p) = -\frac{g_\phi^2}{24\pi} m_\phi^{*2} \beta^3 \left(1 + \frac{12 V_\omega^2 |\mathbf{p}|^2}{\beta^2 m_\phi^{*4}} \right). \quad (67)$$

These expressions agree with those obtained using the covariant form-factor regularization.

IV. MODEL PARAMETERS

In this section, we discuss how the parameters of our model are determined. Important inputs are the in-medium kaon properties, which are obtained from the QMC model [59]. The parameters in the self-energy terms of the effective Lagrangian are fixed using the relevant decay widths [66]. Moreover, each regularization scheme introduces additional parameters that must also be determined.

A. Self-energy parameters

First, we fix the model parameters entering the ϕ -meson self-energy. The vacuum masses of the ϕ meson and kaon are taken as $m_\phi^{\text{expt.}} = 1019.461$ MeV and $m_K^{\text{expt.}} = 493.7$ MeV, respectively. The ϕKK coupling constant is then determined as $g_\phi = 4.517$ by reproducing the decay width of the ϕ meson in vacuum at rest, $\Gamma_\phi^{\text{expt.}} = 4.249$ MeV.

Next, we briefly review the parameters used in the QMC model for the in-medium kaon properties [59]. We use the current quark masses $(m_q, m_s) = (5, 250)$ MeV, with vacuum bag radii $R_N = 0.8$ fm and $R_K = 0.574$ fm for the nucleon and kaon, respectively. The zero-point parameters $z_{N,K} = 3.295$ (the same values within the digits) and the bag constant $B^{1/4} = 170$ MeV are taken to be identical for both hadrons, chosen to reproduce their vacuum properties. In symmetric nuclear matter, the quark-meson coupling constants are fixed to reproduce the saturation point, with a binding energy of 15.7 MeV at $\rho_0 = 0.15$ fm $^{-3}$, yielding $(g_\sigma^q, g_\omega^q) = (5.69, 2.72)$.

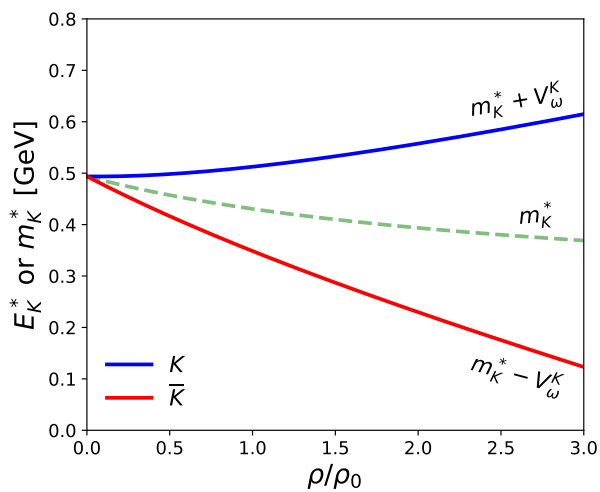


FIG. 2. In-medium mass and energy of a kaon at rest in nuclear matter calculated using the QMC model [59]. The kaon mass shown with green dashed line is reduced by the scalar mean field V_σ , while the kaon–antikaon energy splitting arises from the vector mean field. The kaon energy exhibits a slight repulsion, consistent with experimental observations.

The resulting in-medium kaon energy and effective mass at rest are displayed in Fig. 2. The Lorentz-scalar kaon mass decreases with increasing density due to the attractive scalar mean field V_σ , as indicated by the green dashed line. In contrast, the vector mean field, $V_\omega^K = g_{K\omega}^q \omega$, generates a splitting between kaon and antikaon energies. To account for the slight repulsion observed in the K^+N interaction, of order 20 MeV [67], the quark–vector-meson coupling is phenomenologically enhanced to $g_{K\omega}^q = 1.4^2 g_\omega^q$. We note that alternative mechanisms [68] could also produce a similar repulsive effect without modifying the coupling strength g_ω^q . At normal nuclear matter density, the kaon effective mass is reduced by approximately 13% [59], slightly larger than reported in Ref. [47].

B. Regularization parameters

Lastly, we will describe how the parameters are fixed in both regularization schemes.

a. Form factor regularization In the covariant form factor scheme, two parameters must be fixed: the cutoff Λ and the bare mass m_ϕ^0 in Eq. (27). To illustrate the model uncertainty, we consider $\Lambda = 0.8, 0.9,$ and 1.0 GeV, with the corresponding bare masses $m_\phi^0 = 1.113, 1.164,$ and 1.220 GeV chosen to reproduce the physical ϕ mass in vacuum. These cutoffs are smaller than in the three-momentum form factor scheme [53] because the covariant form factor regulates both \mathbf{q} and q^0 , providing stronger suppression at large momenta.

b. Dimensional regularization In this scheme, two parameters must be fixed: the renormalization scale μ and the subtraction constant $a(\mu)$. The bare mass m_ϕ^0 is set to the physical ϕ mass in vacuum, and the parameters are determined by requiring $\text{Re } \Pi = 0$ at vacuum. Unlike the form factor scheme, variations in m_ϕ^0 can effectively be absorbed into $a(\mu)$. Instead of fixing μ to the kaon mass, we explore several values of $\mu = 0.5, 0.6,$ and 0.7 GeV, with corresponding $a(\mu) = -1.581, -1.216,$ and -0.908 , slightly different from the previous work [47] because a constant term is retained rather than fully absorbed into $a(\mu)$ (See App. B for details).

V. RESULTS AND DISCUSSION

In this section, we present the numerical results on the in-medium behavior of the ϕ meson. We first examine medium-induced modifications to its mass and width at rest using two different regularization schemes. We then extend the analysis to the case of a ϕ meson propagating with finite momentum, which constitutes the main focus of the present work. Finally, we discuss the resulting unpolarized spectral functions and its implications for experiments [41–45].

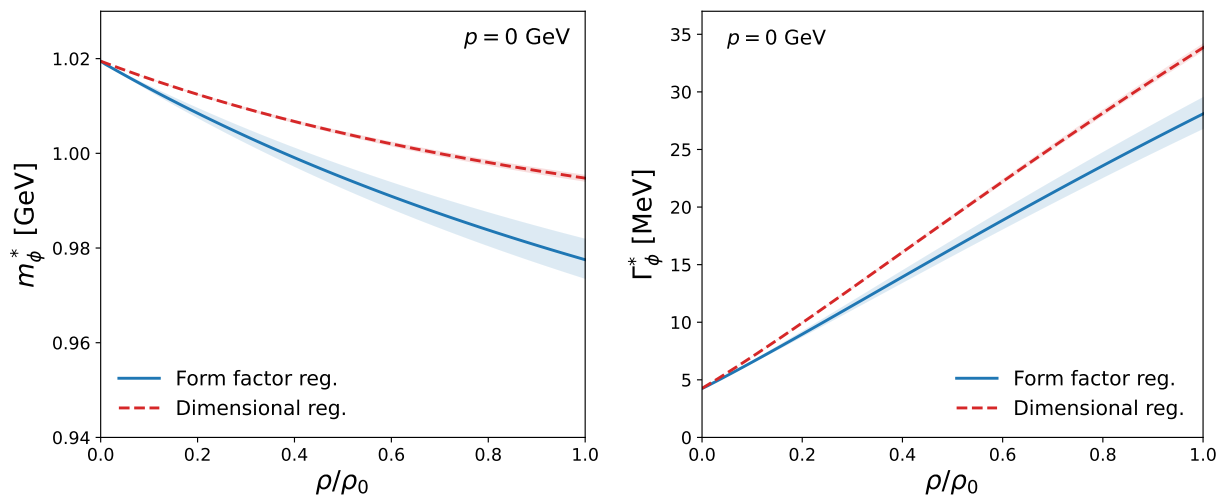


FIG. 3. In-medium mass and width of the ϕ meson at rest as functions of nuclear density, computed using two different regularization schemes. Both approaches exhibit qualitatively similar density dependencies.

A. In-medium properties at rest

We first examine the in-medium ϕ -meson mass and width at rest for densities up to normal nuclear density ρ_0 , relevant to experiments such as those at J-PARC. At zero momentum, the longitudinal and transverse modes are degenerate. Figure 3 displays the density dependence of the in-medium mass m_ϕ^* and width Γ_ϕ^* obtained with both the form-factor and dimensional-regularization schemes. The band represents the dependence on the cutoff parameter $\Lambda=0.8-1.0$ GeV or the renormalization scale $\mu=0.5-0.7$ GeV. With increasing density, the ϕ -meson mass decreases and its width is strongly enhanced, consistent with Refs. [47, 53]. We also note that contact interaction terms significantly affect the in-medium properties at rest, enhancing the downward mass shift while reducing the decay width. Quantitatively, at normal nuclear density ρ_0 , we find a mass reduction of about 2–4% (around 25–40 MeV) and a width broadening by roughly around 30–35 MeV. The large broadening agrees with the recent KEK-E325 analysis [25], while the mass shift is slightly larger although still compatible with earlier results [35].

Figure 3 also shows that, in the form-factor scheme, the mass shift depends strongly on the cutoff values, with larger Λ leading to stronger mass reductions. However, the results in dimensional regularization are relatively insensitive to the renormalization scale. This is because a shift in μ can be partially absorbed into the subtraction constant $a(\mu)$. Despite quantitative differences, both schemes exhibit qualitatively similar density dependencies for the mass and width. Dimensional regularization generally yields slightly weaker medium modifications and a milder scale dependence; however, its results can be reproduced within the form-factor scheme by adopting a smaller Λ .

B. In-medium mass at finite momentum

We now examine the momentum dependence of the in-medium ϕ -meson mass for both polarization modes, which become distinct in nuclear matter. Figure 4 shows the density dependence of the longitudinal-mode mass at fixed momenta $p = 0, 1, 2,$ and 3 GeV. Results obtained with two different regularization schemes display qualitatively similar behavior, although the cutoff dependence becomes more pronounced at finite momentum, as shown by the band, indicating enhanced sensitivity to ultraviolet contributions.

Figure 5 illustrates the momentum dependence of the in-medium mass shift at normal nuclear density. A clear difference between the two modes is observed: while the longitudinal-mode mass decreases quadratically with increasing momentum p , the transverse-mode mass remains constant, showing no noticeable momentum dependence relative to its value at rest. In the present approach, the transverse mode does not couple to the vector mean field at leading order [see Eq. (47)]. The longitudinal mode, however, couples through derivative-type interactions [Eq. (48)], which naturally generate a momentum-dependent contribution to the self-energy. As the ϕ meson momentum increases, this coupling strengthens the medium effect, leading to an enhanced separation between longitudinal and transverse modes. In vacuum, where the vector mean field vanishes, both polarizations remain degenerate for all momenta.

For comparison, this momentum dependence of the longitudinal-mode mass is qualitatively consistent with the QCDSR analysis of Ref. [58]. However, our results for the transverse mode deviate from the QCDSR prediction, which suggests an approximately quadratic increase in mass. In QCDSR, this mode separation originates from the finite density behavior of Lorentz violating condensates. Specifically, as shown in Fig. 3 of Ref. [58], the

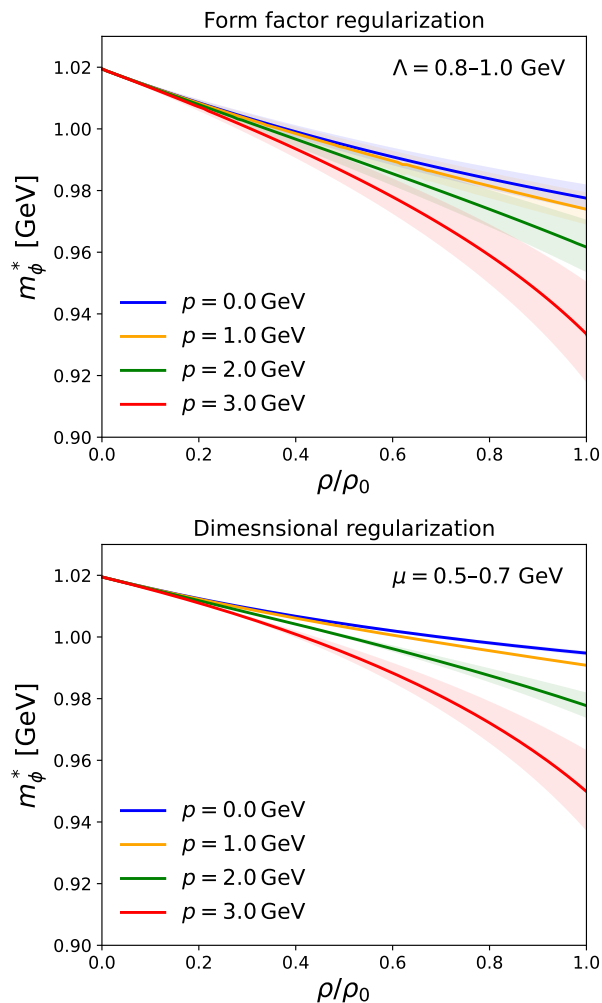


FIG. 4. In-medium mass of the longitudinal-mode ϕ meson as a function of nuclear density at momenta $p = 0, 1, 2,$ and 3 GeV, computed using two different regularization scheme. The transverse-mode mass remains identical to that of the ϕ meson at rest.

longitudinal mass is dominated by a decreasing trend, whereas the transverse mass involves a competition between quark and gluon condensates. Although the net result in QCDSR is an increasing mass, this prediction is subject to larger uncertainties than the longitudinal one.

C. In-medium width at finite momentum

We next discuss the behavior of the in-medium decay width. Figure 6 shows the density dependence of the longitudinal-mode decay width at finite momenta, calculated using two different regularization schemes, without the Lorentz γ factor. Both schemes yield qualitatively consistent results, indicating that the predicted in-medium broadening is robust against the choice of ultraviolet regularization, although quantitatively the results

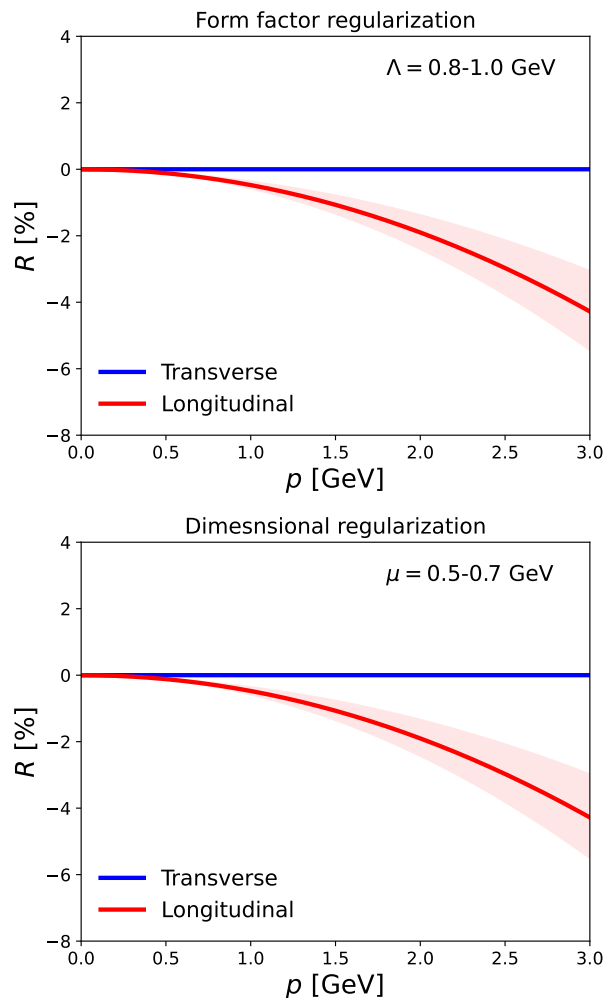


FIG. 5. Momentum dependence p of the in-medium ϕ meson mass ratio $R \equiv \Delta m_\phi^*(p)/m_\phi^*(0)$ (in percentage), where $\Delta m_\phi^*(p) = m_\phi^*(p) - m_\phi^*(0)$, at normal nuclear density for the longitudinal and transverse modes.

depend on the details of the cutoff and scale parameters.

At rest, the width for both modes increases significantly with increasing density. For finite momenta, although the longitudinal width continues to increase with density, its slope gradually decreases as the ϕ -meson momentum increases. This behavior is primarily driven by the momentum-dependent modification of the longitudinal-mode ϕ -meson mass, which reduces the available decay phase space at higher momenta. In contrast, the explicit \mathbf{p}^2 -dependent corrections in Eq. (58) contribute only minor effects in this case. The transverse-mode width, on the other hand, remains essentially identical to its value at rest, consistent with the negligible momentum dependence of the transverse mass.

Figure 7 presents the corresponding results including the Lorentz γ factor. In vacuum, both the transverse and longitudinal decay widths decrease with increasing momentum due to time dilation. Consequently, even in the

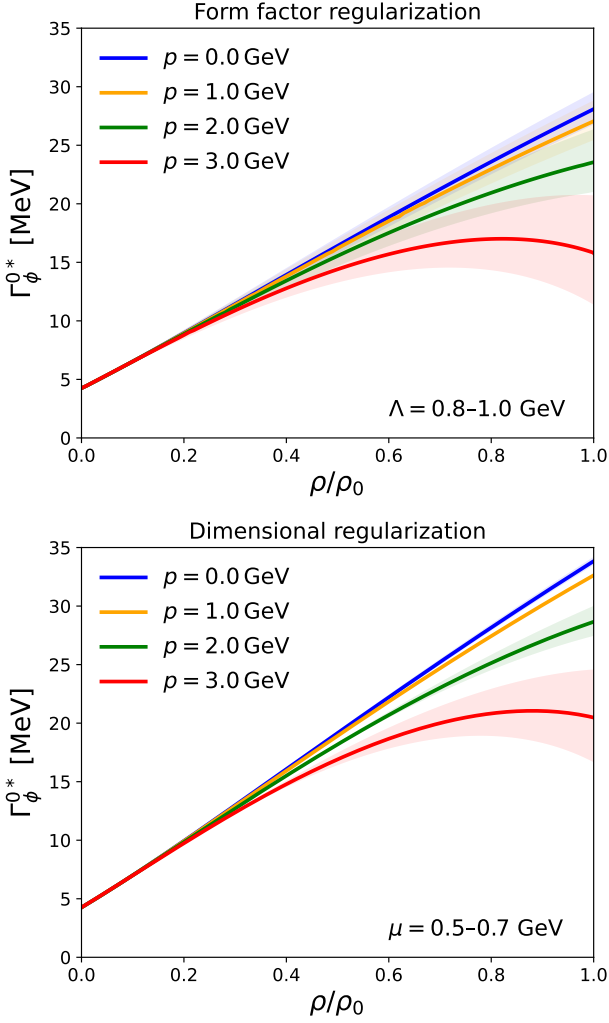


FIG. 6. In-medium width of the longitudinal-mode ϕ meson as a function of nuclear density at momenta $p = 0, 1, 2,$ and 3 GeV, calculated without the Lorentz γ factor using two different regularization schemes. The transverse-mode width in medium remains identical to that of the ϕ meson at rest.

absence of medium effects, the decay widths at finite momentum are reduced compared to their rest-frame values. In the nuclear medium, the competition between intrinsic in-medium broadening and Lorentz time dilation leads to a nontrivial momentum dependence of the decay widths. As a result, at finite momenta, the in-medium transverse decay width also differs from its rest-frame value, despite the absence of intrinsic momentum dependence in the transverse self-energy. The separation between longitudinal and transverse widths becomes increasingly pronounced at higher densities and momenta, reflecting the polarization-dependent nature of the medium modifications.

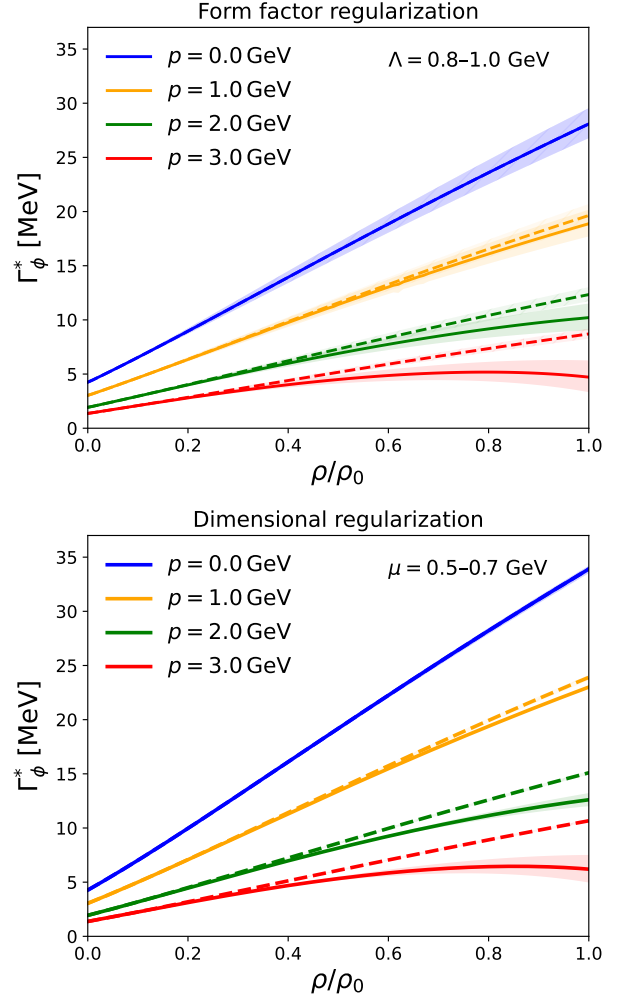


FIG. 7. In-medium width of the ϕ meson as a function of nuclear density at momenta $p = 0, 1, 2,$ and 3 GeV, including the Lorentz γ factor. Note that in vacuum, the width decreases with increasing momentum due to time dilation. The solid and dashed lines represent the results for the longitudinal and transverse modes, respectively.

D. Unpolarized spectral functions

Finally, we examine the unpolarized spectral functions of the ϕ meson at normal nuclear density ρ_0 , shown in Fig. 8. The gray dotted lines represent the vacuum spectral functions, while the blue lines show the in-medium results. For demonstration, we present the results obtained using dimensional regularization.

At $|\mathbf{p}| = 0$, the longitudinal and transverse spectral functions are identical. The nuclear medium induces substantial broadening and a moderate downward mass shift, resulting in a significant redistribution of spectral strength toward lower energies. At finite momenta, $|\mathbf{p}| = 1$ and 2 GeV, the spectral functions of the longitudinal and transverse modes start to split due to polarization-dependent medium effects. However, be-

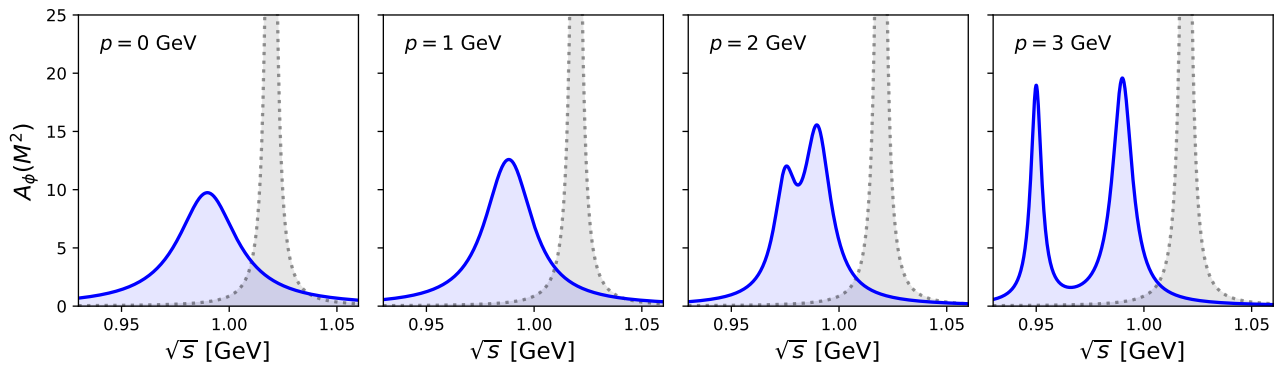


FIG. 8. Unpolarized spectral functions of the ϕ meson at normal nuclear density for momenta $p = 0, 1, 2,$ and 3 GeV, calculated using dimensional regularization. The gray dotted lines represent the vacuum results, while the blue line corresponds to the in-medium spectral function.

cause the two modes still strongly overlap, the resulting unpolarized spectral function exhibits a single broad peak. Starting with momenta around $|\mathbf{p}| = 2$ GeV, a small two-peak structure begins to emerge.

For higher momentum, the widths of the transverse and longitudinal modes become clearly different, as shown in Fig. 7. In the unpolarized spectral function, the transverse contribution appears with a factor of two. However, because the longitudinal mode has a narrower width, its peak height becomes comparable to that of the transverse mode despite the larger transverse weight. As the momentum increases further, the separation between the two modes becomes more pronounced. At $|\mathbf{p}| = 3$ GeV, the longitudinal and transverse peaks are well separated, producing a clear double-peak structure in the spectral function.

Compared to the previous QCDSR analysis [58], an important difference emerges. In that work, the transverse mass increases quadratically with momentum, leading to peak separation already at $|\mathbf{p}| = 1.5\text{-}2.0$ GeV [58]. In contrast, in our model the transverse mode remains unchanged, and a well-separated double-peak structure only appears at around $|\mathbf{p}| = 2.0\text{-}3.0$ GeV. In experiments, however, the situation is more subtle, because the medium effect weakens at higher momenta, as the ϕ meson tends to decay outside the nucleus. It remains to be seen whether a suitable momentum window exists for observing separated peaks in the spectral function.

Furthermore, the E325 experiment observed finite-density effects only for dileptons with $\beta\gamma = |\mathbf{p}|/m_\phi \lesssim 1.25$ [25, 35]. In this kinematic region, our results indicate that the longitudinal and transverse peaks remain strongly overlapping, implying that only a single broadened peak should be observed. Although the longitudinal and transverse mass peaks strongly overlap for $|\mathbf{p}| \lesssim 2$ GeV, measurements of the angular distributions in the $\phi \rightarrow K\bar{K}$ decay channel [60] in the future J-PARC E88/Sa ϕ re experiment [45] may allow the two modes to be disentangled and their respective masses to be extracted. Observation of such polarization-

dependent mass splitting in nuclear matter would constitute a clear signal of Lorentz-symmetry violation induced by the medium.

VI. CONCLUSION AND OUTLOOK

In this work, we studied the in-medium properties of the ϕ meson in the quark-meson coupling (QMC) model [59], incorporating self-consistent kaon mass modifications and kaon-loop contributions [53]. We explored the density and momentum dependence of the ϕ meson mass, width, and spectral functions, emphasizing polarization effects and assessing model dependence using covariant form factor and dimensional regularization schemes.

At normal nuclear density, the kaon effective mass decreases by about 13% [59], inducing a moderate downward mass shift of the ϕ meson by 2-4% and an enhancement of its decay width by a factor of 7-8. The qualitative results are robust against variations in the regularization scheme and consistent with previous studies [47, 53]. For a more rigorous description, additional effects, such as coupled channels, should be included [52].

At finite momentum, a pronounced polarization dependence emerges. While the transverse mode remains insensitive to momentum, the longitudinal mode exhibits a quadratic decrease of the in-medium mass, driven by vector mean fields and derivative interactions, leading to growing polarization splitting with increasing momentum and density. The decay width also shows interesting behavior, with a nontrivial momentum dependence arising from the interplay of intrinsic medium broadening and Lorentz time dilation, producing significant polarization splitting and, at high momentum, a characteristic double-peak structure in the spectral function [58].

Finally, our results can be further tested in future experiments at J-PARC. In the kinematic regime of current measurements, such as KEK E325, the polarization modes overlap, producing a single broadened peak.

At higher momenta, however, our model predicts a substantial polarization splitting, which is partially different from that obtained in a QCDSR approach [58]. Future measurements at J-PARC, such as E88/Sa ϕ re, will help to disentangle this model dependence through angular correlations in the $\phi \rightarrow K\bar{K}$ channel. Moreover, similar in-medium polarization splitting has also been proposed for the K_1^\pm meson [69, 70]. Observation of these effects would provide direct evidence of Lorentz-symmetry breaking in nuclear matter.

ACKNOWLEDGMENT

This work was supported by the RCNP Collaboration Research Network Program under Project No. COREnet 057. A.J.A. benefited from discussions at the Reimei Workshop on In-Medium Modification of Vector Mesons held at Yonsei University and acknowledges the support and hospitality. A.J.A. was supported by the JAEA Postdoctoral Fellowship Program and partly by the PUTI Q1 Grant from the University of Indonesia under Contract No. PKS-206/UN2.RST/HKP.05.00/2025. K.T. was supported by Conselho Nacional de Desenvolvimento Científico e Tecnológico (CNPq, Brazil), Processes No. 304199/2022-2, and FAPESP Process No. 2023/07313-6, and his work was also part of the projects, Instituto Nacional de Ciência e Tecnologia, Nuclear Physics and Applications (INCT-FNA), Brazil, Processes No. 464898/2014-5 and No 408419/2024-5. P.G. is supported by JSPS KAKENHI Grant Numbers JP22H00122 and JP25H00400.

Appendix A: Form factor regularization

In this appendix, we provide the calculational details of the self-energy with the form factor regularization. Especially, the separate contributions of the loop and contact terms for the longitudinal and transverse polarization. In addition, we also provide the explicit analytical expressions.

For the loop contribution $\Pi_{\text{loop}}^\lambda$ given in Eq. (45), the propagators in the self-energy can be rewritten as

$$\begin{aligned} \frac{1}{D_\Lambda^2 D_K^* D_K^*} &= 6 \int_0^1 dx \int_0^{1-x} dy \\ &\quad \times \frac{(1-x-y)}{[D_\Lambda + x(D_K^* - D_\Lambda) + y(D_K^* - D_\Lambda)]^4} \\ &= 6 \int_0^1 dx \int_0^{1-x} dy \frac{(1-x-y)}{([q-xp]^2 + C + i\epsilon)^4}, \end{aligned} \quad (\text{A1})$$

where

$$C = x(1-x)m_\phi^{*2} - (x+y)m_K^{*2} - (1-x-y)\Lambda^2. \quad (\text{A2})$$

To complete the square and ensure that the integration depends only on the kaon loop momentum, we perform the shift $q^\mu \rightarrow q^\mu + xp^\mu$. Using these ingredients, the ϕ -meson self-energy becomes

$$\begin{aligned} \Pi_{\text{loop}}^\lambda(p) &= 12ig_\phi^2(\Lambda^2 - m_K^{*2})^2 \int_0^1 dx \int_0^{1-x} dy \\ &\quad \times (1-x-y) \int \frac{d^4q}{(2\pi)^4} \frac{\mathcal{O}_{\text{loop}}^{\lambda*}}{(q^2 + C)^4}. \end{aligned} \quad (\text{A3})$$

We note that the denominator contains no explicit $|\mathbf{p}|$ dependence; any momentum dependence arises solely from the numerator $\mathcal{O}_{\text{loop}}^{\lambda*}$.

For the transverse mode, Eq. (A3) reduces to

$$\begin{aligned} \Pi_{\text{loop}}^T(p) &= 24ig_\phi^2(\Lambda^2 - m_K^{*2})^2 \int_0^1 dx \int_0^{1-x} dy \\ &\quad \times (1-x-y) \left[\int \frac{d^4q}{(2\pi)^4} \frac{\mathbf{q}_\perp^2}{(q^2 + C)^4} \right]. \end{aligned} \quad (\text{A4})$$

After performing the Wick rotation and carrying out the four-momentum integration in Euclidean space, the self-energy becomes

$$\Pi_{\text{loop}}^T(p) = N \int_0^1 dx \int_0^{1-x} dy \frac{(1-x-y)}{C}, \quad (\text{A5})$$

with $N = g_\phi^2(\Lambda^2 - m_K^{*2})^2/4\pi^2$. For the longitudinal mode, the self-energy reads

$$\begin{aligned} \Pi_{\text{loop}}^L(p) &= \frac{48ig_\phi^2(\Lambda^2 - m_K^{*2})^2}{m_\phi^{*2}} \int_0^1 dx \int_0^{1-x} dy (1-x-y) \\ &\quad \times \left[\int \frac{d^4q}{(2\pi)^4} \frac{([q^0 - V_\omega]|\mathbf{p}| - q^z E_\phi^*)^2}{(q^2 + C)^4} \right]. \end{aligned} \quad (\text{A6})$$

Following the same procedure, we obtain

$$\begin{aligned} \Pi_{\text{loop}}^L(p) &= N \int_0^1 dx \int_0^{1-x} dy (1-x-y) \\ &\quad \times \left(\frac{1}{C} - \frac{2|\mathbf{p}|^2 V_\omega^2}{m_\phi^{*2} C^2} \right). \end{aligned} \quad (\text{A7})$$

Here, a quadratic dependence on the ϕ -meson momentum appears, originating from the derivative coupling in the ϕKK interaction. We emphasize that the second term vanishes both in the vacuum ($V_\omega = 0$) and in the rest frame ($\mathbf{p} = 0$). In these limits, the longitudinal and transverse self-energies coincide, ensuring the correct limiting behavior.

Next, we consider the contribution from the contact diagram, Π_{con}^λ , which is given by

$$\Pi_{\text{con}}^\lambda(p) = 4ig_\phi^2(\Lambda^2 - m_K^{*2})^2 \int \frac{d^4q}{(2\pi)^4} \frac{1}{D_\Lambda^2 D_K^*}. \quad (\text{A8})$$

This contribution is identical for both transverse and longitudinal polarizations. The propagators can be rewritten as

$$\frac{1}{D_\Lambda^2 D_K^*} = 2 \int_0^1 dx \frac{x}{[xD_\Lambda + (1-x)D_K^*]^3} \quad (\text{A9})$$

$$= 2 \int_0^1 dx \frac{x}{(q^2 + E)^3}, \quad (\text{A10})$$

with $E = x\Lambda^2 - (1-x)m_K^{*2}$. The self-energy is then given by

$$\Pi_{\text{con}}^\lambda(p) = 8ig_\phi^2(\Lambda^2 - m_K^{*2})^2 \int_0^1 dx \int \frac{d^4q}{(2\pi)^4} \frac{x}{(q^2 + E)^3}. \quad (\text{A11})$$

After Feynman parameterization and Wick rotation, the contact contribution becomes

$$\Pi_{\text{con}}^\lambda(p) = -\frac{g_\phi^2(\Lambda^2 - m_K^{*2})^2}{4\pi^2} \int dx \frac{x}{E}. \quad (\text{A12})$$

1. Analytical expressions

Here, we provide the analytic expressions for the form factor regularization.

a. Contact term First of all, the self-energy of the contact term in Eqs. (51) and (50) is computed as

$$\Pi_{\text{con}}^\lambda(p) = -N \int \frac{xdx}{x\Lambda^2 - (1-x)m_K^{*2}}, \quad (\text{A13})$$

where the analytic result is given by

$$\Pi_{\text{con}}^\lambda(p) = -\frac{N}{(\Lambda^2 + m_K^{*2})} \left[1 + \frac{m_K^{*2}}{\Lambda^2 + m_K^{*2}} \ln\left(\frac{\Lambda^2}{m_K^{*2}}\right) \right]. \quad (\text{A14})$$

b. \mathbf{p} -independent loop term The self-energy of the loop term common to the longitudinal and transverse modes in Eqs. (51) and (50) for the \mathbf{p} -independent part is given by

$$\Pi_{\text{loop}}^{T/L}(p) = N \int_0^1 dx \int_0^{1-x} dy \frac{(1-x-y)}{C}. \quad (\text{A15})$$

In the region of $2m_K^* < m_\phi^* < \Lambda + m_K^*$, we obtain the real part of the self-energy analytically as

$$\begin{aligned} \text{Re } \Pi_{\text{loop}}^{T/L}(p) &= \frac{N}{12m_\phi^2 \delta^2} \left[\Theta_1 + 2\beta^3 \ln\left(\frac{1+\beta}{1-\beta}\right) \right. \\ &\quad \left. + \gamma \Theta_2 \left\{ \tan^{-1}\left(\frac{\delta_\pm}{\gamma}\right) + \tan^{-1}\left(\frac{\delta_-}{\gamma}\right) \right\} \right. \\ &\quad \left. + \Theta_3 \ln\left(\frac{\delta_K}{\delta_L}\right) \right], \end{aligned} \quad (\text{A16})$$

where we have defined

$$\delta_K = m_K^{*2}/m_\phi^{*2}, \quad \delta = \delta_K - \delta_L, \quad (\text{A17})$$

$$\delta_L = \Lambda^2/m_\phi^{*2}, \quad \delta_\pm = 1 \pm \delta, \quad (\text{A18})$$

and

$$\beta = \sqrt{1 - 4\delta_K}, \quad (\text{A19})$$

$$\gamma = \sqrt{-1 + 2(\delta_K + \delta_L) - (\delta_K - \delta_L)^2}. \quad (\text{A20})$$

To simplify further, we have also defined

$$\Theta_1 = 2\delta[1 - 2\delta], \quad (\text{A21})$$

$$\Theta_2 = 2[2\delta^2 + 5\delta_K - \delta_L - 1], \quad (\text{A22})$$

$$\Theta_3 = [2\delta^3 + 3\delta^2 - 6\delta_K + 1]. \quad (\text{A23})$$

In the same region of $2m_K^* < m_\phi^* < \Lambda + m_K^*$, the imaginary part is obtained as

$$\text{Im } \Pi_{\text{loop}}^{L/T}(p) = -\frac{g_\phi^2}{24\pi} m_\phi^{*2} \beta^3. \quad (\text{A24})$$

c. \mathbf{p} -dependent loop term Now, we compute the second integral in Eq. (51), that is related to the \mathbf{p} -dependent part for the longitudinal mode, defined as Π_{loop}^{L2} . The self-energy is given by

$$\Pi_{\text{loop}}^{L2}(p) = -N_2 |\mathbf{p}|^2 \int_0^1 dx \int_0^{1-x} dy \frac{(1-x-y)}{C^2}, \quad (\text{A25})$$

with $N_2 = 2NV_\omega^2/m_\phi^{*2}$.

In the region of $2m_K^* < m_\phi^* < \Lambda + m_K^*$, the real part is analytically given by

$$\begin{aligned} \text{Re } \Pi_{\text{loop}}^{L2}(p) &= -\frac{N_2 |\mathbf{p}|^2}{m_\phi^{*4} \delta^2} \left[-\beta \ln\left(\frac{1+\beta}{1-\beta}\right) - \frac{1}{2} \ln\left(\frac{\delta_K}{\delta_L}\right) \right. \\ &\quad \left. - \frac{\Theta_4}{\gamma} \left\{ \tan^{-1}\left(\frac{\delta_\pm}{\gamma}\right) + \tan^{-1}\left(\frac{\delta_-}{\gamma}\right) \right\} \right], \end{aligned} \quad (\text{A26})$$

with $\Theta_4 = 1 - 3\delta_K - \delta_L$. In the same region, the imaginary part is obtained as

$$\text{Im } \Pi_{\text{loop}}^{L2}(p) = -\frac{g_\phi^2}{2\pi} \frac{\beta V_\omega^2}{m_\phi^{*2}} |\mathbf{p}|^2. \quad (\text{A27})$$

Appendix B: Dimensional regularization

In this approach, the ϕ -meson self-energy can be written as

$$\Pi_{\text{total}}^\lambda(p) = 2ig_\phi^2 \int \frac{d^4q}{(2\pi)^4} \left[\frac{\mathcal{O}_{\text{loop}}^{\lambda*}}{D_K^* D_K^*} + \frac{\mathcal{O}_{\text{con}}^{\lambda*}}{D_K^*} \right], \quad (\text{B1})$$

without the need of a form factor. For the loop contribution, we introduce Feynman parameters,

$$\frac{1}{D_K^* D_K^*} = \int_0^1 dx \frac{1}{[xD_K^* + (1-x)D_K^*]^2}, \quad (\text{B2})$$

and shift the loop momentum $q^\mu \rightarrow q^\mu + (1-x)p^\mu$, which leads to

$$\Pi_{\text{loop}}^\lambda(p) = 2ig_\phi^2 \int_0^1 dx \int \frac{d^4 q}{(2\pi)^4} \frac{\mathcal{O}_{\text{loop}}^{\lambda*}}{(q^2 - \Delta^* + i\epsilon)^2}, \quad (\text{B3})$$

where $\Delta^* = m_K^{*2} - x(1-x)m_\phi^{*2}$. For the contact term, the Feynman parameter is not needed.

1. Transverse mode

Including both the loop and contact contributions, the transverse self-energy can be written as

$$\Pi_{\text{total}}^T(p) = 4ig_\phi^2 \int \frac{d^d q}{(2\pi)^d} \left[\int_0^1 dx \frac{P_{\mu\nu}^T q^\mu q^\nu}{D_\Delta^{*2}} + \frac{1}{D_K^*} \right], \quad (\text{B4})$$

where, working in d dimensions, we have used the identity $\mathbf{q}_\perp^2 = P_{\mu\nu}^T q^\mu q^\nu$. The momentum integrals are evaluated using dimensional regularization in $d = 4 - \epsilon$ dimensions. Using the standard integral relations

$$\int \frac{d^d q}{(2\pi)^d} \frac{q^\mu q^\nu}{(q^2 - \Delta)^2} = \frac{-ig^{\mu\nu}}{2(4\pi)^{d/2}} \Gamma\left(1 - \frac{d}{2}\right) \Delta^{\frac{d}{2}-1}, \quad (\text{B5})$$

$$\int \frac{d^d q}{(2\pi)^d} \frac{1}{q^2 - \Delta} = \frac{-i}{(4\pi)^{d/2}} \Gamma\left(1 - \frac{d}{2}\right) \Delta^{\frac{d}{2}-1}, \quad (\text{B6})$$

the contact and loop contributions to the transverse self-energy become

$$\Pi_{\text{con}}^T(p) = \frac{4g_\phi^2}{(4\pi)^{d/2}} \Gamma\left(1 - \frac{d}{2}\right) (m_K^{*2})^{\frac{d}{2}-1}. \quad (\text{B7})$$

$$\Pi_{\text{loop}}^T(p) = -\frac{4g_\phi^2 \Gamma(1 - \frac{d}{2})}{(4\pi)^{d/2}} \left[\int_0^1 dx (\Delta^*)^{\frac{d}{2}-1} - (m_K^{*2})^{\frac{d}{2}-1} \right], \quad (\text{B8})$$

where we have used $g^{\mu\nu} P_{\mu\nu}^T = -2$. Expanding around $d = 4 - \epsilon$, we use $(4\pi)^{-d/2} = (4\pi)^{-2} (1 + \frac{\epsilon}{2} \ln 4\pi)$, $\Gamma(1 - \frac{d}{2}) = -\frac{2}{\epsilon} - 1 + \gamma_E$ and $\Delta^{\frac{d}{2}-1} = \Delta [1 - \frac{\epsilon}{2} \ln \Delta]$. Adding the contact term, the renormalized transverse self-energy reads

$$\Pi_{\text{loop}}^T(p) = -\frac{g_\phi^2}{4\pi^2} \int_0^1 dx \left(\Delta^* \ln \frac{\Delta^*}{\mu^2} - m_K^{*2} \ln \frac{m_K^{*2}}{\mu^2} - a(\mu) \frac{m_\phi^2}{6} \right), \quad (\text{B9})$$

where the first two terms arise from the loop and contact contributions, respectively. The real part of the transverse self-energy can be evaluated analytically as

$$\text{Re } \Pi_{\text{total}}^T(p) = -\frac{g_\phi^2}{4\pi^2} \left[-\frac{m_\phi^{*2}}{6} \left(\beta^3 \ln \left(\frac{1+\beta}{1-\beta} \right) + \frac{8m_K^{*2}}{m_\phi^{*2}} + \ln \frac{m_K^{*2}}{\mu^2} - \frac{5}{18} \right) - a(\mu) \frac{m_\phi^2}{6} \right] \quad (\text{B10})$$

with $\beta = \sqrt{1 - 4m_K^{*2}/m_\phi^{*2}}$. Note that in Ref. [47], the constant $5/18$ was absorbed into $a(\mu)$. However, we retain it here for consistency with the numerical integration of the first term in Eq. (B9).

2. Longitudinal mode

For the longitudinal mode, the loop contribution is given by

$$\Pi_{\text{loop}}^L(p) = \frac{8ig_\phi^2}{m_\phi^{*2}} \int_0^1 dx \int \frac{d^4 q}{(2\pi)^4} \frac{([q^0 - V_\omega]|\mathbf{p}| - q^z E_\phi^*)^2}{(q^2 - \Delta^*)^2}. \quad (\text{B11})$$

Since the cross term vanishes by symmetry, the expression reduces to

$$\mathcal{O}_{\text{loop}}^L = \frac{4}{m_\phi^{*2}} \left((q^z)^2 E_\phi^{*2} + (q^0)^2 |\mathbf{p}|^2 + |\mathbf{p}|^2 V_\omega^2 \right). \quad (\text{B12})$$

After performing the Wick rotation and extending the integration to d dimensions, we use

$$(q^z)^2 = \frac{1}{d} q_E^2, \quad (q^0)^2 = -\frac{1}{d} q_E^2, \quad (\text{B13})$$

where q_E denotes the Euclidean four-momentum. This yields

$$\mathcal{O}_{\text{loop}}^L = \frac{m_\phi^{*2}}{d} q_E^2 + |\mathbf{p}|^2 V_\omega^2. \quad (\text{B14})$$

The longitudinal loop contribution then becomes

$$\Pi_{\text{loop}}^L(p) = -\frac{8g_\phi^2}{m_\phi^{*2}} \int_0^1 dx \int \frac{d^d q_E}{(2\pi)^d} \frac{\frac{m_\phi^2}{d} q_E^2 + |\mathbf{p}|^2 V_\omega^2}{(q_E^2 + \Delta^*)^2}. \quad (\text{B15})$$

Using the standard Euclidean integrals

$$\int \frac{d^d q_E}{(2\pi)^d} \frac{1}{(q_E^2 + \Delta)^2} = \frac{1}{(4\pi)^{d/2}} \Gamma\left(2 - \frac{d}{2}\right) \Delta^{\frac{d}{2}-2}, \quad (\text{B16})$$

$$\int \frac{d^d q_E}{(2\pi)^d} \frac{q_E^2}{(q_E^2 + \Delta)^2} = \frac{1}{(4\pi)^{d/2}} \frac{d}{2} \Gamma\left(1 - \frac{d}{2}\right) \Delta^{\frac{d}{2}-1}. \quad (\text{B17})$$

and combining the loop and contact contributions, we obtain

$$\begin{aligned} \Pi_{\text{total}}^L(p) = & -\frac{g_\phi^2}{4\pi^2} \int_0^1 dx \left[\Delta^* \ln \frac{\Delta^*}{\mu^2} - m_K^{*2} \ln \frac{m_K^{*2}}{\mu^2} \right. \\ & \left. - 2V_\omega^2 \frac{|\mathbf{p}|^2}{m_\phi^{*2}} \left(\ln \frac{\Delta^*}{\mu^2} + 1 \right) - a(\mu) \frac{m_\phi^2}{6} \right]. \end{aligned} \quad (\text{B18})$$

Note that the \mathbf{p} -dependent part also exhibits a μ depen-

dence. The real part can be evaluated analytically as

$$\begin{aligned} \text{Re } \Pi_{\text{total}}^L(p) = & -\frac{g_\phi^2}{4\pi^2} \left[-\frac{m_\phi^{*2}}{6} \left(\beta^3 \ln \left(\frac{1+\beta}{1-\beta} \right) + \frac{8m_K^{*2}}{m_\phi^{*2}} \right. \right. \\ & \left. \left. + \ln \frac{m_K^{*2}}{\mu^2} - \frac{8}{15} \right) - a(\mu) \frac{m_\phi^2}{6} \right. \\ & \left. - 2V_\omega^2 \frac{|\mathbf{p}|^2}{m_\phi^{*2}} \left(\ln \frac{m_K^{*2}}{\mu^2} - 1 + \beta \ln \frac{1+\beta}{1-\beta} \right) \right]. \end{aligned} \quad (\text{B19})$$

For the imaginary part, the results are identical to those obtained using the form-factor regularization, and we therefore do not discuss them further here.

-
- [1] G. E. Brown and M. Rho, Chiral restoration in hot and/or dense matter, *Phys. Rept.* **269**, 333 (1996), [arXiv:hep-ph/9504250](#).
- [2] S. Leupold, V. Metag, and U. Mosel, Hadrons in strongly interacting matter, *Int. J. Mod. Phys. E* **19**, 147 (2010), [arXiv:0907.2388 \[nucl-th\]](#).
- [3] R. S. Hayano and T. Hatsuda, Hadron properties in the nuclear medium, *Rev. Mod. Phys.* **82**, 2949 (2010), [arXiv:0812.1702 \[nucl-ex\]](#).
- [4] G. E. Brown and M. Rho, Scaling effective Lagrangians in a dense medium, *Phys. Rev. Lett.* **66**, 2720 (1991).
- [5] T. Hatsuda and S. H. Lee, QCD sum rules for vector mesons in the nuclear medium, *Phys. Rev. C* **46**, R34 (1992).
- [6] P. Gubler and K. Ohtani, Constraining the strangeness content of the nucleon by measuring the ϕ meson mass shift in nuclear matter, *Phys. Rev. D* **90**, 094002 (2014), [arXiv:1404.7701 \[hep-ph\]](#).
- [7] P. Gubler and W. Weise, Phi meson spectral moments and QCD condensates in nuclear matter, *Nucl. Phys. A* **954**, 125 (2016), [arXiv:1602.09126 \[hep-ph\]](#).
- [8] J. Kim, P. Gubler, and S. H. Lee, ϕ meson properties in nuclear matter from QCD sum rules with chirally separated four-quark condensates, *Phys. Rev. D* **105**, 114053 (2022), [arXiv:2204.11440 \[hep-ph\]](#).
- [9] S. Durr *et al.*, Lattice computation of the nucleon scalar quark contents at the physical point, *Phys. Rev. Lett.* **116**, 172001 (2016), [arXiv:1510.08013 \[hep-lat\]](#).
- [10] Y.-B. Yang, A. Alexandru, T. Draper, J. Liang, and K.-F. Liu (xQCD), π N and strangeness sigma terms at the physical point with chiral fermions, *Phys. Rev. D* **94**, 054503 (2016), [arXiv:1511.09089 \[hep-lat\]](#).
- [11] A. Abdel-Rehim, C. Alexandrou, M. Constantinou, K. Hadjiyiannakou, K. Jansen, C. Kallidonis, G. Koutsou, and A. Vaquero Aviles-Casco (ETM), Direct Evaluation of the Quark Content of Nucleons from Lattice QCD at the Physical Point, *Phys. Rev. Lett.* **116**, 252001 (2016), [arXiv:1601.01624 \[hep-lat\]](#).
- [12] S. Borsanyi, Z. Fodor, C. Hoelbling, L. Lellouch, K. K. Szabo, C. Torrero, and L. Varnhorst, Ab-initio calculation of the proton and the neutron's scalar couplings for new physics searches, (2020), [arXiv:2007.03319 \[hep-lat\]](#).
- [13] G. S. Bali, S. Collins, P. Georg, D. Jenkins, P. Korcyl, A. Schäfer, E. E. Scholz, J. Simeth, W. Söldner, and S. Weishäupl (RQCD), Scale setting and the light baryon spectrum in $N_f = 2 + 1$ QCD with Wilson fermions, *JHEP* **05**, 035, [arXiv:2211.03744 \[hep-lat\]](#).
- [14] Y. Aoki *et al.* (Flavour Lattice Averaging Group (FLAG)), FLAG review 2024, *Phys. Rev. D* **113**, 014508 (2026), [arXiv:2411.04268 \[hep-lat\]](#).
- [15] Y.-S. Oh and H. C. Bhang, Asymmetries in phi photoproduction and the OZI violation, *Phys. Rev. C* **64**, 055207 (2001), [arXiv:nucl-th/0104068](#).
- [16] S.-H. Kim, T. S. H. Lee, S.-i. Nam, and Y. Oh, Dynamical model of ϕ meson photoproduction on the nucleon and He4, *Phys. Rev. C* **104**, 045202 (2021), [arXiv:2108.12039 \[nucl-th\]](#).
- [17] Y. Lyu, T. Doi, T. Hatsuda, Y. Ikeda, J. Meng, K. Sasaki, and T. Sugiura, Attractive N- ϕ interaction and two-pion tail from lattice QCD near physical point, *Phys. Rev. D* **106**, 074507 (2022), [arXiv:2205.10544 \[hep-lat\]](#).
- [18] L. M. Abreu, P. Gubler, K. P. Khemchandani, A. Martinez Torres, and A. Hosaka, A study of the ϕ N correlation function, *Phys. Lett. B* **860**, 139175 (2025), [arXiv:2409.05170 \[hep-ph\]](#).
- [19] V. Metag, M. Nanova, and E. Y. Paryev, Meson-nucleus potentials and the search for meson-nucleus bound states, *Prog. Part. Nucl. Phys.* **97**, 199 (2017), [arXiv:1706.09654 \[nucl-ex\]](#).
- [20] L. Tolos and L. Fabbietti, Strangeness in Nuclei and Neutron Stars, *Prog. Part. Nucl. Phys.* **112**, 103770 (2020), [arXiv:2002.09223 \[nucl-ex\]](#).
- [21] W. Cassing and E. L. Bratkovskaya, Parton-Hadron-String Dynamics: an off-shell transport approach for relativistic energies, *Nucl. Phys. A* **831**, 215 (2009), [arXiv:0907.5331 \[nucl-th\]](#).
- [22] P. Muhlich, T. Falter, C. Greiner, J. Lehr, M. Post, and U. Mosel, Photoproduction of phi mesons from nuclei, *Phys. Rev. C* **67**, 024605 (2003), [arXiv:nucl-th/0210079](#).
- [23] P. Gubler, M. Ichikawa, T. Song, and E. Bratkovskaya, Production and in-medium modification of φ mesons in proton-nucleus reactions from a transport approach, *Phys. Rev. C* **111**, 034908 (2025), [arXiv:2408.15364 \[hep-ph\]](#).
- [24] G. Balassa, K. Aoki, P. Gubler, S. H. Lee, H. Sako, and G. Wolf, Studying the In-Medium φ Meson Spectrum Through Kaons in Proton-Nucleus Reactions, *PTEP* **2025**, 113C01 (2025), [arXiv:2508.11344 \[hep-ph\]](#).

- [25] M. Ichikawa *et al.* (KEK-PS E325), Analysis of Spectral Modification of φ Mesons at Finite Density Using a Transport Approach in 12 GeV pA Reactions, *PTEP* **2025**, 093D01 (2025), [arXiv:2507.00420 \[nucl-ex\]](#).
- [26] C. M. Ko and B. H. Sa, Phi meson production in hadronic matter, *Phys. Lett. B* **258**, 6 (1991).
- [27] W. S. Chung, G.-Q. Li, and C. M. Ko, Phi meson production in heavy ion collisions at SIS energies, *Nucl. Phys. A* **625**, 347 (1997), [arXiv:nucl-th/9704002](#).
- [28] W. S. Chung, C. M. Ko, and G.-Q. Li, Seeing phi meson through the dilepton spectra in heavy ion collisions, *Nucl. Phys. A* **641**, 357 (1998), [arXiv:nucl-th/9803059](#).
- [29] S. Pal, C. M. Ko, and Z.-w. Lin, Phi meson production in relativistic heavy ion collisions, *Nucl. Phys. A* **707**, 525 (2002), [arXiv:nucl-th/0202086](#).
- [30] B. B. Back *et al.* (E917), Production of phi mesons in Au+Au collisions at 11.7-A-GeV/c, *Phys. Rev. C* **69**, 054901 (2004), [arXiv:nucl-ex/0304017](#).
- [31] B. I. Abelev *et al.* (STAR), Measurements of phi meson production in relativistic heavy-ion collisions at RHIC, *Phys. Rev. C* **79**, 064903 (2009), [arXiv:0809.4737 \[nucl-ex\]](#).
- [32] T. Song, J. Aichelin, and E. Bratkovskaya, In-medium effects in ϕ meson production in heavy-ion collisions from subthreshold to relativistic energies, *Phys. Rev. C* **106**, 024903 (2022), [arXiv:2205.10251 \[nucl-th\]](#).
- [33] J. Steinheimer, T. Reichert, and M. Bleicher, Determination of the ϕ -meson production process and its absorption cross section via directed flow, *Phys. Lett. B* **869**, 139870 (2025), [arXiv:2507.19289 \[hep-ph\]](#).
- [34] T. Ishikawa *et al.*, phi photo-production from Li, C, Al, and Cu nuclei at $E(\gamma) = 1.5$ GeV to 2.4 GeV, *Phys. Lett. B* **608**, 215 (2005), [arXiv:nucl-ex/0411016](#).
- [35] R. Muto *et al.* (KEK-PS-E325), Evidence for in-medium modification of the phi meson at normal nuclear density, *Phys. Rev. Lett.* **98**, 042501 (2007), [arXiv:nucl-ex/0511019](#).
- [36] F. Sakuma *et al.* (E325), Study of nuclear matter modification of decay widths in $\phi \rightarrow e^+e^-$ and $\phi \rightarrow K^+K^-$ channels, *Phys. Rev. Lett.* **98**, 152302 (2007), [arXiv:nucl-ex/0606029](#).
- [37] M. H. Wood *et al.* (CLAS), Absorption of the ω and ϕ Mesons in Nuclei, *Phys. Rev. Lett.* **105**, 112301 (2010), [arXiv:1006.3361 \[nucl-ex\]](#).
- [38] A. Polyanskiy *et al.*, Measurement of the in-medium phi-meson width in proton-nucleus collisions, *Phys. Lett. B* **695**, 74 (2011), [arXiv:1008.0232 \[nucl-ex\]](#).
- [39] M. Hartmann *et al.*, Momentum dependence of the phi-meson nuclear transparency, *Phys. Rev. C* **85**, 035206 (2012), [arXiv:1201.3517 \[nucl-ex\]](#).
- [40] J. Adamczewski-Musch *et al.* (HADES), Strong absorption of hadrons with hidden and open strangeness in nuclear matter, *Phys. Rev. Lett.* **123**, 022002 (2019), [arXiv:1812.03728 \[nucl-ex\]](#).
- [41] S. Yokkaichi *et al.*, Electron pair spectrometer at the J-PARC 50-GeV PS to explore the chiral symmetry in QCD (2007).
- [42] M. Naruki, Hadron physics at J-PARC, *PTEP* **2012**, 02B013 (2012).
- [43] K. Aoki *et al.*, Experimental Study of In-medium Spectral Change of Vector Mesons at J-PARC, *Few Body Syst.* **64**, 63 (2023).
- [44] K. Aoki *et al.*, Experimental investigation of vector mesons in medium through dielectron decay at J-PARC, *J. Subatomic Part. Cosmol.* **3**, 100019 (2025).
- [45] H. Sako *et al.*, Experimental studies of in-medium modification of ϕ meson mass through $\phi \rightarrow K^+K^-$ decays, *J. Subatomic Part. Cosmol.* **1-2**, 100012 (2024).
- [46] J. G. Messchendorp *et al.*, Hadron Physics Opportunities at FAIR, (2025), [arXiv:2512.15986 \[hep-ex\]](#).
- [47] C. M. Ko, P. Levai, X. J. Qiu, and C. T. Li, Phi meson in dense matter, *Phys. Rev. C* **45**, 1400 (1992).
- [48] M. Asakawa and C. M. Ko, Phi meson mass in hot and dense matter, *Nucl. Phys. A* **572**, 732 (1994).
- [49] F. Klingl, T. Waas, and W. Weise, Modification of the phi meson spectrum in nuclear matter, *Phys. Lett. B* **431**, 254 (1998), [arXiv:hep-ph/9709210](#).
- [50] S. Zschocke, O. P. Pavlenko, and B. Kampfer, Evaluation of QCD sum rules for light vector mesons at finite density and temperature, *Eur. Phys. J. A* **15**, 529 (2002), [arXiv:nucl-th/0205057](#).
- [51] D. Cabrera and M. J. Vicente Vacas, Phi meson mass and decay width in nuclear matter, *Phys. Rev. C* **67**, 045203 (2003), [arXiv:nucl-th/0205075](#).
- [52] D. Cabrera, A. N. Hiller Blin, and M. J. Vicente Vacas, ϕ meson self-energy in nuclear matter from ϕN resonant interactions, *Phys. Rev. C* **95**, 015201 (2017), [arXiv:1609.03880 \[nucl-th\]](#).
- [53] J. J. Cobos-Martínez, K. Tsushima, G. Krein, and A. W. Thomas, ϕ meson mass and decay width in nuclear matter and nuclei, *Phys. Lett. B* **771**, 113 (2017), [arXiv:1703.05367 \[nucl-th\]](#).
- [54] Z. Ahmad, N. Chahal, A. Kumar, and S. Dutt, Impact of Finite Volume on Kaon, Antikaon, and ϕ Meson Masses and Decay Widths in Asymmetric Strange Hadronic Matter, *PTEP* **2025**, 013B03 (2025), [arXiv:2407.05263 \[hep-ph\]](#).
- [55] A. Mondal and A. Mishra, ϕ meson in nuclear matter and atomic nuclei, *Phys. Rev. D* **111**, 094037 (2025), [arXiv:2502.08320 \[nucl-th\]](#).
- [56] M. Kaur and A. Kumar, ϕ meson properties in dense resonance matter at finite temperature, *Phys. Rev. D* **112**, 014030 (2025), [arXiv:2505.07065 \[hep-ph\]](#).
- [57] S. H. Lee, Vector mesons in-medium with finite three momentum, *Phys. Rev. C* **57**, 927 (1998), [Erratum: *Phys.Rev.C* 58, 3771 (1998)], [arXiv:nucl-th/9705048](#).
- [58] H. Kim and P. Gubler, The ϕ meson with finite momentum in a dense medium, *Phys. Lett. B* **805**, 135412 (2020), [arXiv:1911.08737 \[hep-ph\]](#).
- [59] K. Tsushima, K. Saito, A. W. Thomas, and S. V. Wright, In-medium kaon and antikaon properties in the quark meson coupling model, *Phys. Lett. B* **429**, 239 (1998), [Erratum: *Phys.Lett.B* 436, 453–453 (1998)], [arXiv:nucl-th/9712044](#).
- [60] I. W. Park, H. Sako, K. Aoki, P. Gubler, and S. H. Lee, Disentangling longitudinal and transverse modes of the ϕ meson through dilepton and kaon decays, *Phys. Rev. D* **107**, 074033 (2023), [arXiv:2211.16949 \[hep-ph\]](#).
- [61] C. Gale and J. I. Kapusta, Vector dominance model at finite temperature, *Nucl. Phys. B* **357**, 65 (1991).
- [62] P. A. M. Guichon, A Possible Quark Mechanism for the Saturation of Nuclear Matter, *Phys. Lett. B* **200**, 235 (1988).
- [63] K. Saito, K. Tsushima, and A. W. Thomas, Nucleon and hadron structure changes in the nuclear medium and impact on observables, *Prog. Part. Nucl. Phys.* **58**, 1 (2007), [arXiv:hep-ph/0506314](#).
- [64] P. A. M. Guichon, J. R. Stone, and A. W. Thomas,

- Quark–Meson-Coupling (QMC) model for finite nuclei, nuclear matter and beyond, *Prog. Part. Nucl. Phys.* **100**, 262 (2018), [arXiv:1802.08368 \[nucl-th\]](#).
- [65] G. E. Brown, C. M. Ko, and K. Kubodera, Strangeness production in relativistic heavy ion collisions, *Z. Phys. A* **341**, 301 (1992).
- [66] S. Navas *et al.* (Particle Data Group), Review of particle physics, *Phys. Rev. D* **110**, 030001 (2024).
- [67] C. Fuchs, Kaon production in heavy ion reactions at intermediate energies, *Prog. Part. Nucl. Phys.* **56**, 1 (2006), [arXiv:nucl-th/0507017](#).
- [68] A. J. Arifi, P. T. P. Hutaaruk, and K. Tsushima, In-medium properties of the light and heavy-light mesons in a light-front quark model, *Phys. Rev. D* **107**, 114010 (2023), [arXiv:2302.12382 \[hep-ph\]](#).
- [69] I. W. Park, H. Sako, K. Aoki, P. Gubler, and S. H. Lee, Identifying the transverse and longitudinal modes of the K^* and K_1 mesons through their angular-dependent decay modes, *Phys. Rev. D* **109**, 114042 (2024), [arXiv:2403.18288 \[hep-ph\]](#).
- [70] S. Yeo, H. Kim, and S. H. Lee, K_1^\pm mesons moving in nuclear matter, *Phys. Rev. D* **110**, 014013 (2024), [arXiv:2404.04532 \[nucl-th\]](#).